Asymmetric branching of dissociated photofragments of HD^+ in an intense femtosecond laser field

Souvik Chatterjee,[1] Bibhas Dutta,[2] and S. S. Bhattacharyya[1,*]

[1]*Atomic and Molecular Physics Section, Department of Materials Science, Indian Association for the Cultivation of Science, Jadavpur, Kolkata 700 032, India*

[2]*Sambhunath College, Labpur, Birbhum, West Bengal 731303, India*

(Received 13 April 2011; published 20 June 2011)

We have numerically explored the asymmetry in the branching ratio of the photofragments in the photodissociation of HD^+ (neutral D and neutral H), leading to the possibility of localization of the electron on a chosen nucleus by careful tuning of the laser parameters. For two different frequencies we show that, starting from an initial stationary wave function, proper tuning of the pulse duration (2σ) and peak intensities (I^0) of the laser pulses can lead to very different branching ratios of the two reaction channels. The results are interpreted in terms of the propagation of the nonstationary wave packet through regions having dominant radiative or nonradiative interactions at different times. We also investigate what effect the choice of initial vibrational state has on the overall asymmetry in the branching ratio of the dissociation products.

DOI: 10.1103/PhysRevA.83.063413 PACS number(s): 33.80.Gj, 42.50.Hz

I. INTRODUCTION

Theoretical and experimental studies of behavior of simple molecules in intense pulsed laser fields have revealed many interesting features of nuclear dynamics. Most of these new features cannot be generally predicted on an intuitive basis without detailed numerical computation. Thus computations of molecular dynamics in intense fields continue to remain of fundamental importance, as they can be used to elucidate some very general questions about matter-field interaction. Also such studies have stimulated efforts towards coherent femtosecond control of molecular motion. Such control schemes, in turn, may be of use for the realization of logic gates and design of algorithms in optical quantum computing with atoms and molecules. Optical coherent control technology can be used to create widespread opportunities for manipulation of the final distribution of products in different channels in various chemical reactions, thereby opening pathways for synthesis of products.

Of all possible photoinduced processes in simple molecules, dissociation of diatomics has been one of the earliest to be investigated intensively. Such studies have mostly concentrated on the simplest one-electron species, H_2^+, D_2^+, (as have been reviewed in [1]) and their heteronuclear isotopic analog, HD^+, which in certain respects may show interesting and significantly different features from the corresponding homonuclear counterparts. Some interesting works have also been done on hydrogen halide and alkali metal halide molecule photodissociation. In this context, the main control objective has been to manipulate the final distribution of the fragmentation products in different channels. The development of ultrafast laser technology as well as sophisticated detection methods has now created opportunities for testing of computational proposals for controlling the outcome of dissociative reactions. Such control would require careful tuning of the field parameters such as carrier frequency, peak intensities, and pulse duration and shape, as well as the carrier-envelope phase. In addition, for multipulse schemes, which are now used in various forms in most of the control scenario, interpulse delay time and relative phase of the pulses can be important control parameters. For example, a recent work has discussed how a vibrational wave packet can be launched on the ground electronic state of D_2^+ by tunnel ionization as well as bond softening of neutral D_2 and how the ion yield in the dissociation channel can be modulated by using a second pulse with a variable delay [2].

As far as heteronuclear ions are concerned, the branching ratios of different atomic products produced in the dissociation and dissociative ionization processes are of major interest. A recent example is provided by the work of Korolkov and co-workers [3,4], who numerically solved the coupled Schrödinger equation with a motivation of controlling the ratio of product ion yields D^+/Cl^+ in dissociation of DCl^+ by intense chirped pulses. The sign of the chirp was found to have a significant influence on the D^+/Cl^+ ratio in dissociative ionization of DCl [5].

For the photodissociation of NaI the branching ratio of $Na^*(^2P_{3/2,1/2})$ to $Na(^2S_{1/2})$ was experimentally shown to be controllable by the variation of the timing between two transform-limited ultrafast laser pulses [6]. An alternative way to achieve quantum control of NaI photodissociation reaction product states was shown in [7] by specially tailored ultrafast light fields. Similarly, control of the branching ratio between ground- and excited-state iodine atoms by changing the time delay and relative phase between the pump and control pulse as well as by the chirp was also reported [8]. For NaI the branching ratio between molecular and three-body dissociative photoionization was shown to be controllable in a pump-probe situation. In a time-dependent three-state wave-packet study the durations of the femtosecond pump and probe pulses emerged as major controls of this branching ratio [9]. In [10] a time-dependent quantum wave-packet calculation was used to demonstrate that the relative phase between two intense few-cycle pulses of frequencies ω and 2ω can be used to control the branching ratio of the products

*msssb@iacs.res.in

$I(^2P_{3/2})$ and $I(^2P_{1/2})$ in the photodissociation of HI molecule. Earlier a pump-pump coherent control scheme was used in [11] for manipulating the product branching ratio in the photodissociation of Li_2 into Li(2*s*) + Li(2*p*) and Li(2*s*) + Li(3*p*) channels. Dissociation probability and branching ratio for Br_2 molecule in a femtosecond laser field was studied in [12].

Though made for an atomic system, the study on control of double ionization in the case of Ca [13] is relevant in our context, because in this work a single pulse was employed and its temporal asymmetry was used to steer the atomic system from an initial eigenstate to a double-electron continuum through a coherent superposition of excited states.

In another recent work [14], the main focus of interest was the study of the branching ratios for different photon absorption channels in photodissociative processes in H_2^+ and D_2^+ in an intense ultrashort laser field. The authors demonstrated that these ratios can be controlled by variation of the peak intensity and also the duration of the single laser pulse used. The identification of the multiphoton processes was made primarily from comparison of the nuclear kinetic energy release spectrum with a time-varying Floquet–Born-Oppenheimer calculation.

In the present work our primary objective is the investigation of the asymmetry in the branching ratios of the photofragments of HD^+ between neutral D and neutral H atoms resulting from a single femtosecond pulse and the possibility of control of this ratio through tuning of the pulse parameters.

Some earlier theoretical calculations had indeed reported computational results of the asymmetry in the branching ratio between the two possible dissociation channels in HD^+ within both time-independent and time-dependent frameworks. In [15], a phase-locked (ω, 2ω) laser pulse was used to predict an appreciable isotope separation in the fragmentation of HD^+ as well as to induce asymmetry in the angular distribution of the emitted fragments. Experimental studies in [16,17] of the dissociation of the ground state HD^+ indicates that the lower $H^+ + D$ channel is 7% more likely than the $D^+ + H$ channel. It was demonstrated in [18,19] that dissociation to either of the channels in HD^+ can be made more probable by proper choice of the carrier-envelope phase difference (CEPD) of a single ultrashort laser pulse. The calculations used a three-dimensional model (one nuclear plus two electronic degrees of freedom). More recently, Bhattacharya and Bhattacharyya [20] have reported the near equality of the fluxes in two channels in the photofragmentation of the HD^+ system. Taking the rotational motion of the internuclear axis into account, the branching ratios to different photon absorption channels resulting from two-frequency multiphoton dissociation of HD^+ in the framework of a time-independent calculation were reported along with their angular distribution [21,22]. The control of both electron excitation and localization in the dissociation of the H_2^+, HD^+, and HT^+ is achieved in [23]. In the beginning, an ultraviolet pulse is used for excitation of the electronic wave packet on the dissociative state. A time-delayed near-infrared pulse is then introduced and by adjusting the delay time between the pulses as well as the carrier-envelope phase of the second pulse, effective control over electron localization on one of the dissociating nuclei can be achieved. An alternative multipulse scheme for controlling electron localization on a desired nucleus in D_2^+ through vibrational wave-packet manipulation is proposed in [24]. The second pulse responsible for the electron localization basically operates on a moving wave packet.

We have performed a detailed numerical simulation of the photofragmentation process of HD^+ starting from an initial ground-vibrational-state wave function. The rotational motion has been neglected, as is usually done. Also the usual two-state approach has been invoked and a technique for solution of the Schrödinger equation for the nuclear wave packet in the presence of intense pulsed femtosecond fields has been adopted. The branching ratios to the two channels have been computed, both as a function of intensity as well as that of pulse time for two different frequencies. The two laser frequencies employed for the simulation are the 800-nm fundamental frequency of a Ti sapphire laser and its third harmonic.

The two features that make HD^+ sufficiently different from, and also more interesting than, its homonuclear counterparts H_2^+ and D_2^+ are the presence of strong asymptotically diverging intrinsic dipole moments in both states and the presence of *g*-*u* symmetry-breaking nonadiabatic interaction [25,26]. This nonadiabatic interaction also removes the degeneracy of the molecular states at large distances, which, unlike its homonuclear counterparts, go to different asymptotically distinguishable atomic states D(1*s*) or H(1*s*). The presence of this interaction also results in a transition dipole moment which varies in the large internuclear separation region in a way different from that for the homonuclear species.

The possibility of strongly asymmetrical branching between the asymptotic atomic states can arise because the interplay between the radiative and nonadiabatic interactions largely controls this branching. By changing the intensity and duration of the pulses the nuclear wave packets can be induced to experience these interactions at different times and to different extents, which ultimately for some combinations of intensities and pulse time, leads to different fluxes in the two asymptotic channels. Finally, interpretations of the variation of the branching ratio with the pulse times and intensities for different frequencies have been provided in terms of such interplays of symmetry-breaking nonadiabatic interactions with various radiative interactions through transition and permanent dipole moments at various times on the way to dissociation.

II. THEORY

We investigate the strong-field photodissociation dynamics of HD^+ molecular ion by solving the time-dependent Schrödinger equation in the nuclear coordinates *R*. A four-component nuclear wave function in the basis of the two lowest electronic states has been formed for this purpose. The nuclear wave functions belonging to each electronic state have been subdivided on the basis of their parities (even though the parity-determining quantum number *J* had not been included in the description of the system) [15,20]. In the case of the heteronuclear HD^+ ion, this is useful to account for the permanent dipole-moment-induced intraelectronic radiative couplings, as radiative transitions connect only electronic states belonging to groups with different parities. Thus the

Schrödinger equation in the basis of two electronic G and E states, each with even (e) and odd (o) parities, takes the form

$$i\hbar\frac{\partial}{\partial t}\begin{pmatrix}\Psi_{G_e}(R,t)\\ \Psi_{G_o}(R,t)\\ \Psi_{E_e}(R,t)\\ \Psi_{E_o}(R,t)\end{pmatrix}=\mathrm{H}(R,t)\begin{pmatrix}\Psi_{G_e}(R,t)\\ \Psi_{G_o}(R,t)\\ \Psi_{E_e}(R,t)\\ \Psi_{E_o}(R,t)\end{pmatrix}, \tag{1}$$

with

$$\mathrm{H}=-\frac{\hbar^2}{2m}\frac{\partial^2}{\partial R^2}+V(R,t). \tag{2}$$

Here, m is the reduced mass of the nuclei and R is the internuclear separation. $V(R,t)$ is the potential matrix, in the four-component basis, including both the interatomic potentials and the off-diagonal laser-induced interstate as well as intrastate radiative couplings. The parity of the initial vibrational state can be defined arbitrarily:

$$V(R,t)=\begin{pmatrix}V_{\mathrm{G}}(R) & -\mu_{\mathrm{GG}}(R)\mathrm{E}(t) & 0 & -\mu_{\mathrm{EG}}(R)\mathrm{E}(t)\\ -\mu_{\mathrm{GG}}(R)\mathrm{E}(t) & V_{\mathrm{G}}(R) & -\mu_{\mathrm{EG}(R)}\mathrm{E}(t) & 0\\ 0 & -\mu_{\mathrm{EG}}(R)\mathrm{E}(t) & V_{\mathrm{E}}(R) & -\mu_{\mathrm{EE}}(R)\mathrm{E}(t)\\ -\mu_{\mathrm{EG}}(R)\mathrm{E}(t) & 0 & -\mu_{\mathrm{EE}}(R)\mathrm{E}(t) & V_{\mathrm{E}}(R)\end{pmatrix}. \tag{3}$$

We have used a sine-squared temporal pulse shape, so that

$$E(t)=E^0 f(t)\cos(\omega t), \tag{4}$$

$$f(t)=\sin^2\left\{\frac{\Pi t}{2\sigma}\right\}. \tag{5}$$

E^0 is the peak of the magnitude of the electric field and 2σ is the total pulse duration. $\mu_{\mathrm{G-G}}(R)$ and $\mu_{\mathrm{E-E}}(R)$ are the R-dependent permanent dipole moments and $\mu_{\mathrm{G-E}}(R)$ is the R-dependent transition dipole moments of the HD^+ system. The expression for the transition and permanent dipole matrix elements between the asymptotically correct states in terms of the transition moment between the two lowest Born-Oppenheimer states is shown in [15,20].

The split operator Fourier transform method is employed for solution of this time-dependent Schrödinger equation. The initial stationary wave function with an arbitrary choice of parity at time t_0 is propagated to time t_f using the time evolution operator. The expression for the unitary evolution operator from $t_n{-}1$ to t_n ($t_n{-}t_n{-}1=\delta t$) is

$$\begin{aligned}U(t_n\leftarrow t_{n-1})&=e^{-i\left(\frac{H}{\hbar}\delta t\right)}\\&=e^{i\left(\frac{\hbar}{2m}\frac{\partial^2}{\partial R^2}\frac{\delta t}{2}\right)}e^{-i\left(\frac{V(R,t)\delta t}{\hbar}\right)}e^{i\left(\frac{\hbar}{2m}\frac{\partial^2}{\partial R^2}\frac{\delta t}{2}\right)}.\end{aligned} \tag{6}$$

This expression is correct to second order in δt.

The effect of the application of an exponential operator can be conveniently calculated in the basis that makes the operator diagonal, and this basis must be found at each time. The effects of the propagation on the nuclear wave packet in each time step are calculated separately for the potential and kinetic parts in the bases in which these two operators are diagonal.

The asymptotic atomic states arising from the dissociation of HD^+ are distinguishable and nondegenerate. This nondegeneracy between the molecular orbitals can be accounted for by taking into account the coupling between electronic wave functions of the Born-Oppenheimer $1s\sigma_g$ and $2p\sigma_u$ states through the symmetry-breaking term in the full Hamiltonian arising from the mass asymmetry. At each internuclear separation R the proper basis-state electronic wave functions can be constructed as linear combinations of the Born-Oppenheimer wave functions as shown by Carrington and Kennedy [25]. We can write the nuclear wave functions Ψ_{G} and Ψ_{E} in this proper basis (in which the molecular orbitals asymptotically go to the correct atomic limit) as linear combinations of the nuclear wave functions Φ_g and Φ_u in the Born-Oppenheimer basis [15,20]:

$$\Psi_{\mathrm{G}}(R,t)=a(R)\Phi_g(R,t)+b(R)\Phi_u(R,t), \tag{7}$$

$$\Psi_{\mathrm{E}}(R,t)=-b(R)\Phi_g(R,t)+a(R)\Phi_u(R,t). \tag{8}$$

The coupling coefficients $a(R)$ and $b(R)$ satisfy the unitarity relation, $a^2(R)+b^2(R)=1$. These mixing coefficients a and b, along with the potential energies $V_{\mathrm{G}}(R)$ and $V_{\mathrm{E}}(R)$ of the two new electronic states GS and ES, calculated earlier [25,26], have been used by us. At small internuclear separations, the actual wave functions practically coincide with the Born-Oppenheimer wave functions, giving $a=1$ and $b=0$. However, in the asymptotic limit the actual states describe atomic orbitals, unlike the Born-Oppenheimer states, which denote linear combinations of the two atomic orbitals in equal proportions. Thus in the asymptotic limit the mixing coefficients take the value $a=b=1/\sqrt{2}$.

In our simulation for each step of propagation, the kinetic energy operator is applied in the basis of the proper Born-Oppenheimer states. The wave-packet components are then transformed to the basis (G, E) with correct asymptotic limits $\mathrm{D}(1s)+\mathrm{H}^+$ for G and $\mathrm{H}(1s)+\mathrm{D}^+$ for E [19] for application of the potential propagation operator whose matrix elements are known in this basis. In this way, the R dependences of the mixing coefficients a and b induce nonadiabatic coupling between the two components of the nuclear wave packet. The transformation used for projecting the wave-function components on the G and E electronic basis is given in Eqs. (7) and (8).

The method employed for calculation of the energy spectrum of the photofragments is discussed in detail in [20] and the corresponding parameters were used in the numerical calculations. We have allowed the wave-packet propagation to continue up to 50,000 a.u. of time (206.8 ps).

III. RESULTS AND DISCUSSION

The distribution of photofragments between the two asymptotic channels $H^+ + D(1s)$ and $H(1s) + D^+$ obtained on dissociation of HD^+ has been explored for single femtosecond pulses of different durations and peak intensities. Our motivation is to find the circumstances leading to significant asymmetries of the distribution of photofragments between these two channels and to interpret the mechanism by which these asymmetries can arise with the aim to control the branching ratios by adjusting the parameters of the single pulse. Two different frequencies have been used for this purpose, the fundamental frequency of a 800-nm Ti sapphire laser and its third harmonic with a wavelength of 267 nm. The peak intensities (I^0) of the $\sin^2$ pulses have been varied over an order of magnitude from 10^{14} to 10^{15} W/cm^2. The pulse widths (full temporal duration of the pulses) range from 24 to ~120 fs. At first we present the results for the branching ratios starting from an initial $v = 0$ state which has arbitrarily been assigned an even parity.

In the case of a 267-nm laser, only single-photon dissociation is observed for the entire range of intensities and pulse duration explored. For high-frequency radiation (267 nm) the one-photon crossing between the dressed potentials takes place at a value of R around which the ground-state vibrational wave packet shifts because of the distortion of the potential. This occurs before the three-photon crossing opens up appreciably at a shorter distance.

In Figs. 1(a)–1(d), for a 267-nm-wavelength laser, we show the branching ratios in the two product channels as functions of the pulse time for four different peak intensities. In all the cases, for the shortest pulse ($2\sigma = 24.2$ fs) the flux in the two channels $H^+ + D$ and $D^+ + H$ tends to be equal. However, with the increase of the temporal width of the laser pulse, the channel $H + D^+$ is more favored at all intensities. A maximum branching of fragments in the outgoing $H + D^+$ channel occurs at ~70 fs for $I^0 = 2 \times 10^{14}$W/cm^2 and at ~55 fs for the other values of peak intensities. On further increase of the pulse time, flux in the ground-state channel (which asymptotically goes to the $D + H^+$) increases again. In particular, in the case of $I^0 = 3 \times 10^{14}$W/cm^2 in Fig. 1(b), the dissociation flux in the ground-state channel reaches a maximum of almost 85%, at 89 fs, after which a gradual decline

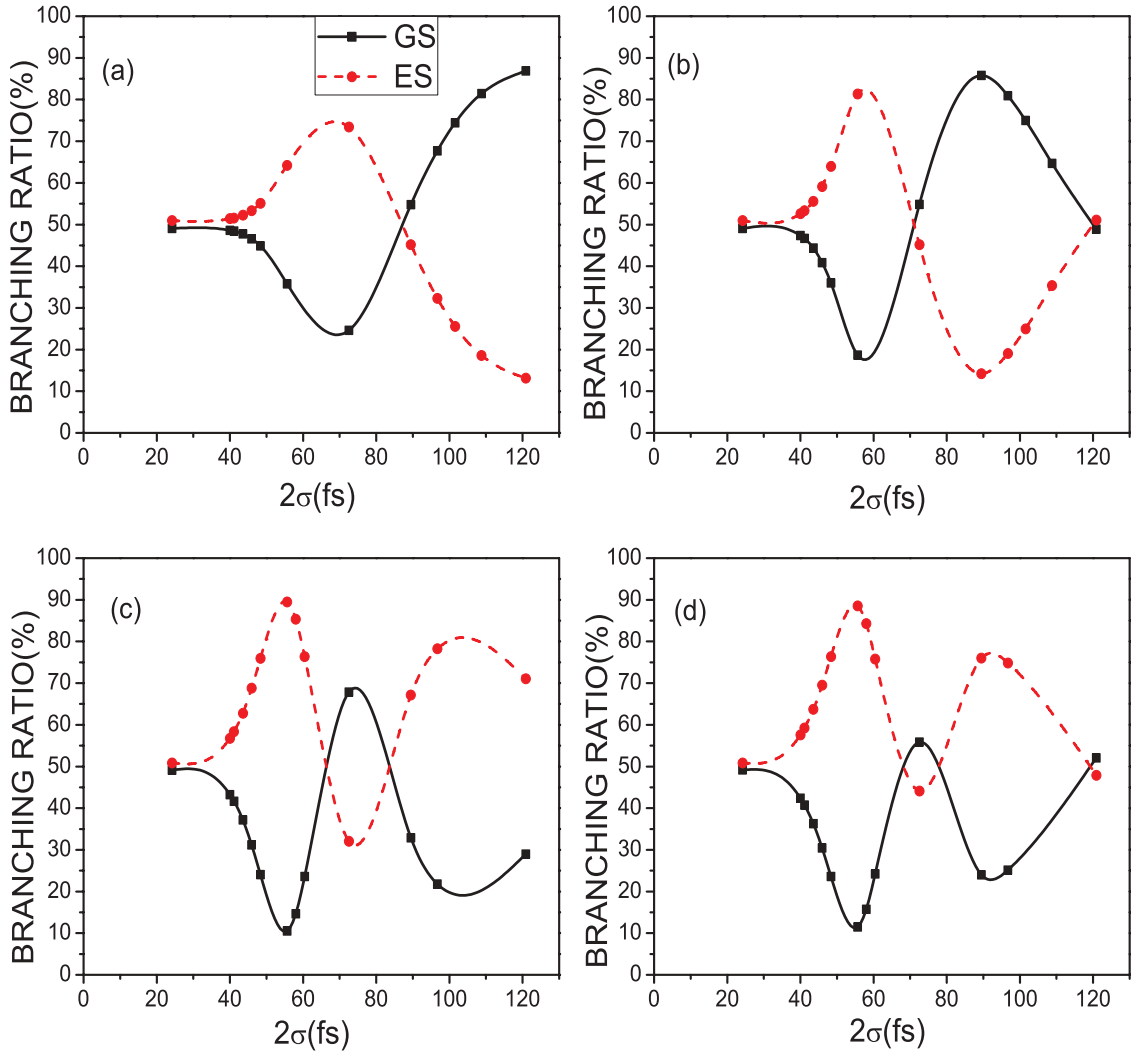

FIG. 1. (Color online) The branching ratios of the photofragments of HD^+ to the GS and ES state channel, for 267-nm-wavelength laser, as functions of pulse time (2σ) for (a) $I^0 = 2\times10^{14}$W/cm^2, (b) $I^0 = 3\times10^{14}$W/cm^2, (c) $I^0 = 5\times10^{14}$W/cm^2, and (d) $I^0 = 6\times10^{14}$W/cm^2

in the branching to this channel is observed on further increase of the pulse duration. For a 120-fs-long pulse, the dissociated photofragments in the two product channels become almost equal again. At still higher intensities, as shown in Figs. 1(c) and 1(d), the relative probability of dissociation through the ground state increases beyond 55 fs and at ∼72 fs becomes higher than that through the excited-state channel. However, further increase of the pulse length causes a second crossing of the branching ratio curves. In the case of $I^0 = 6 \times 10^{14}\mathrm{W/cm^2}$, at a large pulse time of 120 fs the asymmetry in the distribution of the dissociated fragments seems to disappear. Thus it seems that a single pulse can be used to effectively channelize the dissociated fragments into one product atomic state or another through variation of pulse time.

The coupling between states in different regions of R are either radiative (due to either transition or permanent dipole moments) or mainly nonradiative (because of strong R dependence of the mixing coefficients a and b) or both. Variation of the pulse duration actually allows the wave packet to cross different regions of the R space at different times. The transition dipole moment matrix elements between the G and E state plays an important role beyond the equilibrium distance of 2 a.u., and attains a maximum at $R = 10$ a.u. after which it rapidly falls to zero, becoming insignificant at $R = 15$ a.u. The radiative transitions between the two molecular states can take place only when the transition matrix element is significant. The permanent dipole moments show a divergence from $R =$ 9.5 a.u. At large R, the transition dipole moment is practically negligible and the radiative couplings due to permanent dipole moments are very strong. Hence radiative transitions in the large R region take place only between the odd and even components of the same electronic state. The nonadiabatic coupling is effective in a narrow region between 10 and 15 a.u and causes mixing between the same parity components of different electronic states. The wave-packet components experience different electric fields while passing through the same regions of internuclear separation for pulses of different durations. The importance of these different interactions can thus be controlled by pulse-time variation resulting in variation of branching patterns between the two asymptotic atomic channels. The relative importance of the radiative transition and nonradiative mixing can also be controlled to some extent by changing the peak intensity, keeping the pulse shape invariant.

Figures 2(a) and 2(e) show the time evolution of the populations for the ground and excited electronic states in the interaction region (defined as $R < 40$ a.u.) for a peak intensity of $5 \times 10^{14}\mathrm{W/cm^2}$ and for pulse durations of 24.2 and 55.6 fs, respectively. At low pulse time, i.e., for $2\sigma = 24.2$ fs, the population at first is completely transferred to the excited state, but gradually becomes equally distributed in the two electronic states at later times when no radiative coupling is operative. This leads to an almost equal flux distribution in the two reaction channels. Figure 2(e) shows that for the broader pulse also a major part of the population is transferred to the excited state after the pulse has reached the peak. As the wave packet moves outwards a small amount of retransfer takes place but the major part remains on the excited-state channel and dissociates as $H + D^+$. These results can be interpreted on the basis of the wave-packet evolution on the respective potential surfaces involved. Figures 2(b)–2(d) and 2(f)–2(h) show the snapshots of the evolution of the squared components of the wave packet on the ground and excited electronic potentials for two pulses of different durations at the indicated times. As the intensity starts to increase the initial stationary wave function for $v = 0$ on the ground electronic state potential becomes nonstationary and starts shifting outward due to the distortion of the potential. At the same time transfer to the excited state starts to occur due to the influence of the transition moment. In Fig. 2(b) at ∼14.5 fs most of the wave packet has just reached the avoided crossing region around $R = 3$–3.5 a.u., where the transition matrix element is significant and the transfer of wave-packet component to the excited electronic state becomes more important. By the time the pulse ends (24.2 fs) the complete wave packet has moved well beyond the bound region (the dissociation probability is almost unity) and the population transfer has also completed [Fig. 2(c)]. However, as seen from Fig. 2(a), a fraction of the wave packet is transferred from the excited electronic state to the ground electronic state after the pulse is over. The situation at a later time when the wave packet has almost crossed the nonadiabatic coupling region has been shown in Fig. 2(d).The peak position of the wave-packet components present in the ground and excited electronic potentials are the same at this time. In the absence of the laser field we can say that the nonadiabatic coupling, important in the region through which the wave-packet components pass during 24–39 fs, is responsible for the final near equality of the interaction region population in the two electronic states, clearly seen at $t = 38.7$ fs in Fig. 2(d). Because of the involvement of the nonadiabatic interaction the transfer takes place to the odd component of the ground electronic state. When the wave packet escapes the interaction region the proportion of flux in the two atomic channels corresponds to the population in the two electronic states asymptotically going to those atomic states.

Figure 1(c) shows that the peak in the branching ratio asymmetry for $I^0 = 5 \times 10^{14}\mathrm{W/cm^2}$ is attained for a pulse time of ∼55 fs. For a pulse time of this magnitude, the wave packet moves to a somewhat larger distance by the time the laser field strength achieves its peak compared to the case of 24.2-fs pulse. In this case also most of the laser-induced coupling mediated population transfer occurs well after the peak is reached, while the wave-packet components move through the region $R = 3$–8 a.u. This is evident from Fig. 2(f) (where only a small portion of the wave packet has been transferred to the higher electronic state). Further transfer to the excited state occurs while the wave packet continues to move outward; this can be seen in Fig. 2(g) (which shows that almost the entire wave packet resides on the excited state potential by 38.7 fs). The small dip in the population of the excited state shown in Fig. 2(e) occurs, because during the falling region of the pulse, a small portion of the wave packet does make the reverse transition to the ground state through stimulated emission, as can be seen from Fig. 2(h). In contrast to the short-pulse case, the electromagnetic field continues to influence the dynamics of the wave-packet components while the nonadiabatic coupling region is traversed. Thus some radiative transition to the odd ground-state component from the even one may take place in this region apart from some transfer from the odd excited-state components through

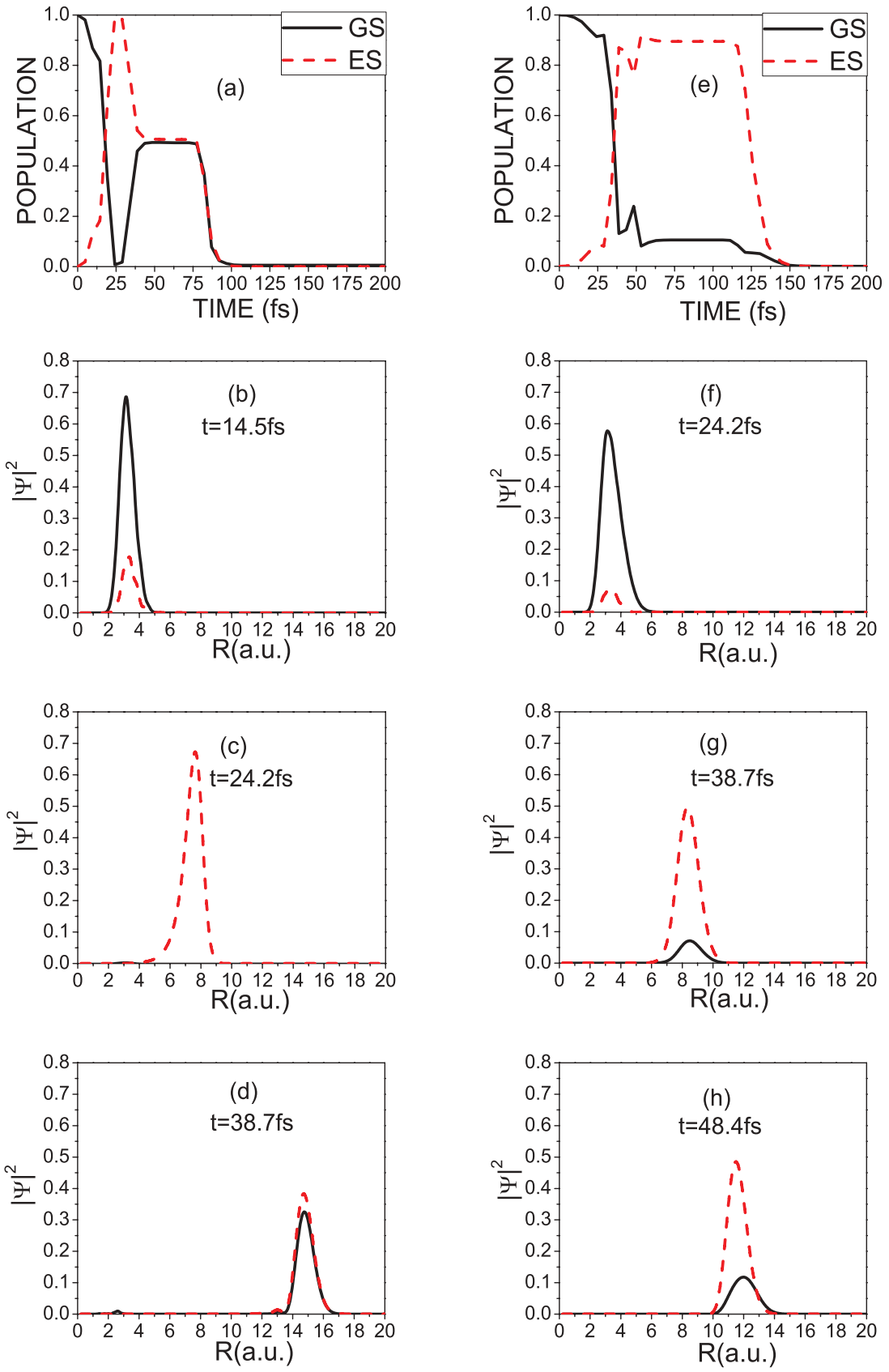

FIG. 2. (Color online) Wave-packet dynamics for $I^0 = 5 \times 10^{14}$ W/cm^2. (a) Population dynamics of the GS and ES states in the interaction region for $2\sigma = 24.2$ fs. (b)–(d) Snapshots of the evolution of the wave-packet components on the two electronic potentials at three different times for $2\sigma = 24.2$ fs. (e) Population dynamics of the GS and ES state in the interaction region for $2\sigma = 55.6$ fs. (f)–(h) Snapshots of the evolution of the wave-packet components on the two electronic potentials at three different times for $2\sigma = 55.6$ fs.

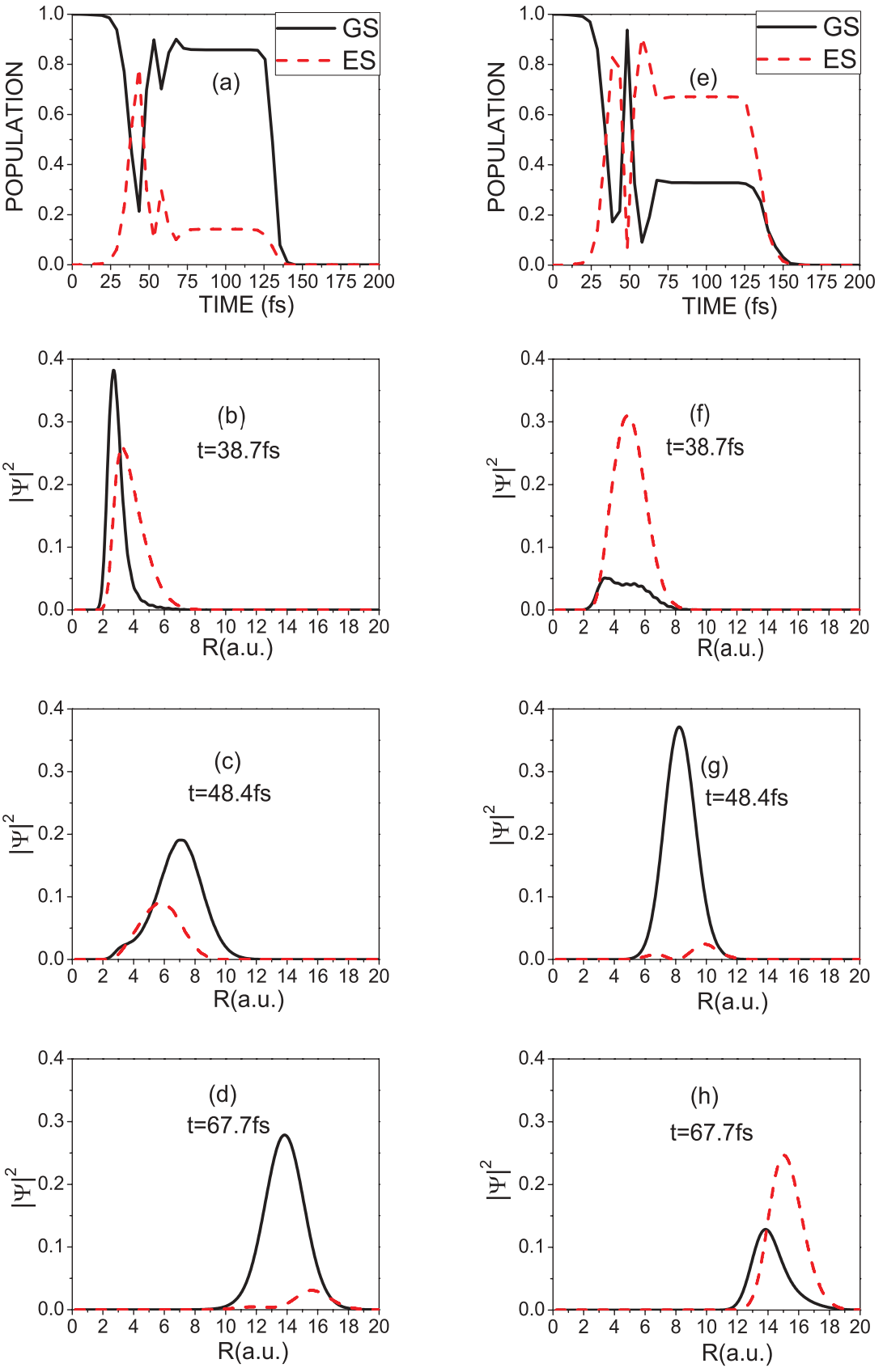

FIG. 3. (Color online) Wave-packet dynamics for $2\sigma = 89.5$ fs. (a) Population dynamics of the GS and ES state in the interaction region for $I^0 = 3 \times 10^{14}$W/cm^2. (b)–(d) Snapshots of the evolution of the wave-packet components on the two electronic potentials at three different times for $I^0 = 3 \times 10^{14}$W/cm^2. (e) Population dynamics of the GS and ES state in the interaction region for $I^0 = 5 \times 10^{14}$W/cm^2. (f)–(h) Snapshots of the evolution of the wave-packet components on the two electronic potentials at three different times for $I^0 = 5 \times 10^{14}$W/cm^2.

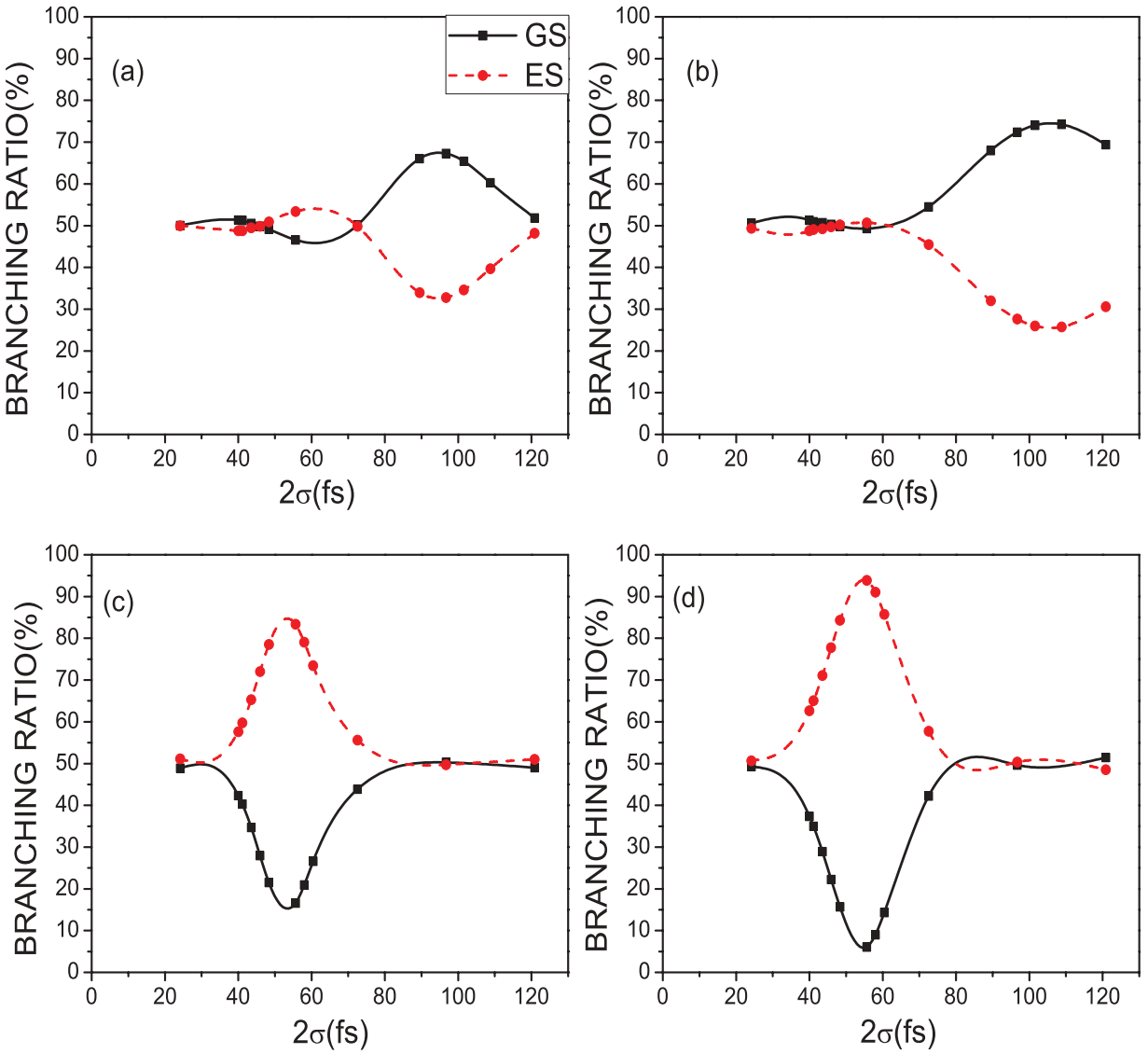

FIG. 4. (Color online) The branching ratios of the photofragments of HD^+ to the GS and ES state channel, for 800-nm-wavelength laser, as functions of pulse time (2σ) for (a) $I^0 = 2 \times 10^{14}\mathrm{W/cm^2}$, (b) $I^0 = 3 \times 10^{14}\mathrm{W/cm^2}$, (c) $I^0 = 5 \times 10^{14}\mathrm{W/cm^2}$, and (d) $I^0 = 6 \times 10^{14}\mathrm{W/cm^2}$

the nonadiabatic coupling. It seems that the presence of a moderate radiative coupling in this large R region prevents complete equalization of the population through nonadiabatic interaction. The influence of the pulse persists in the falling region after 38.7 fs, and influences the final distribution of the completely dissociated flux between the two atomic channels.

Figures 3(a) and 3(e) demonstrate the time evolutions of the population of the GS and ES channels at two different peak intensities, $I^0 = 3 \times 10^{14}\mathrm{W/cm^2}$ and $I^0 = 5 \times 10^{14}\mathrm{W/cm^2}$, respectively, for a pulse time of 89.5 fs. In both cases the population shows oscillation from the GS state to the ES state and back to the GS state within the first 50-fs timescale. In both cases the transfer to the ES state starts at ~25 fs and reaches a maximum of ~80% during the rising portion of the pulse. This transfer takes place in the range of 2–8 a.u., but the maximum is obtained at a slightly earlier time for the higher-intensity pulse. The wave packets have been shown at 38.7 fs for these two pulses [Figs. 3(b) and 3(f)]. After this stage, as the wave-packet components continue to move further right, still remaining in the strong dipole region, a radiative retransfer to the GS (even) state takes place. Figures 3(c) and 3(g) show that a retransfer to the GS state has indeed occurred by 48.4 fs and that the magnitude of this retransfer is certainly greater at higher intensity. At about this time the permanent dipole moment starts playing its role. This is recognized by the fact that the odd component wave packet on the ground state starts building up near the tail at the expense of the even component. Oscillation of the wave packet between two electronic states continues even after 50 fs in the case of the higher-intensity pulse. For the lower intensity, such oscillatory trend is much weaker. For the lower intensity, the norm of the GS state wave packet becomes maximum at ~58 fs, but at that time a significant portion has already been retransferred to the ES state in the higher-intensity case. Thus for the stronger coupling an extra half cycle of population oscillation between the two electronic states takes place. For even higher intensities there will be even more oscillations between the GS and ES states within this region. The wave packet crosses the 10–12 a.u. region

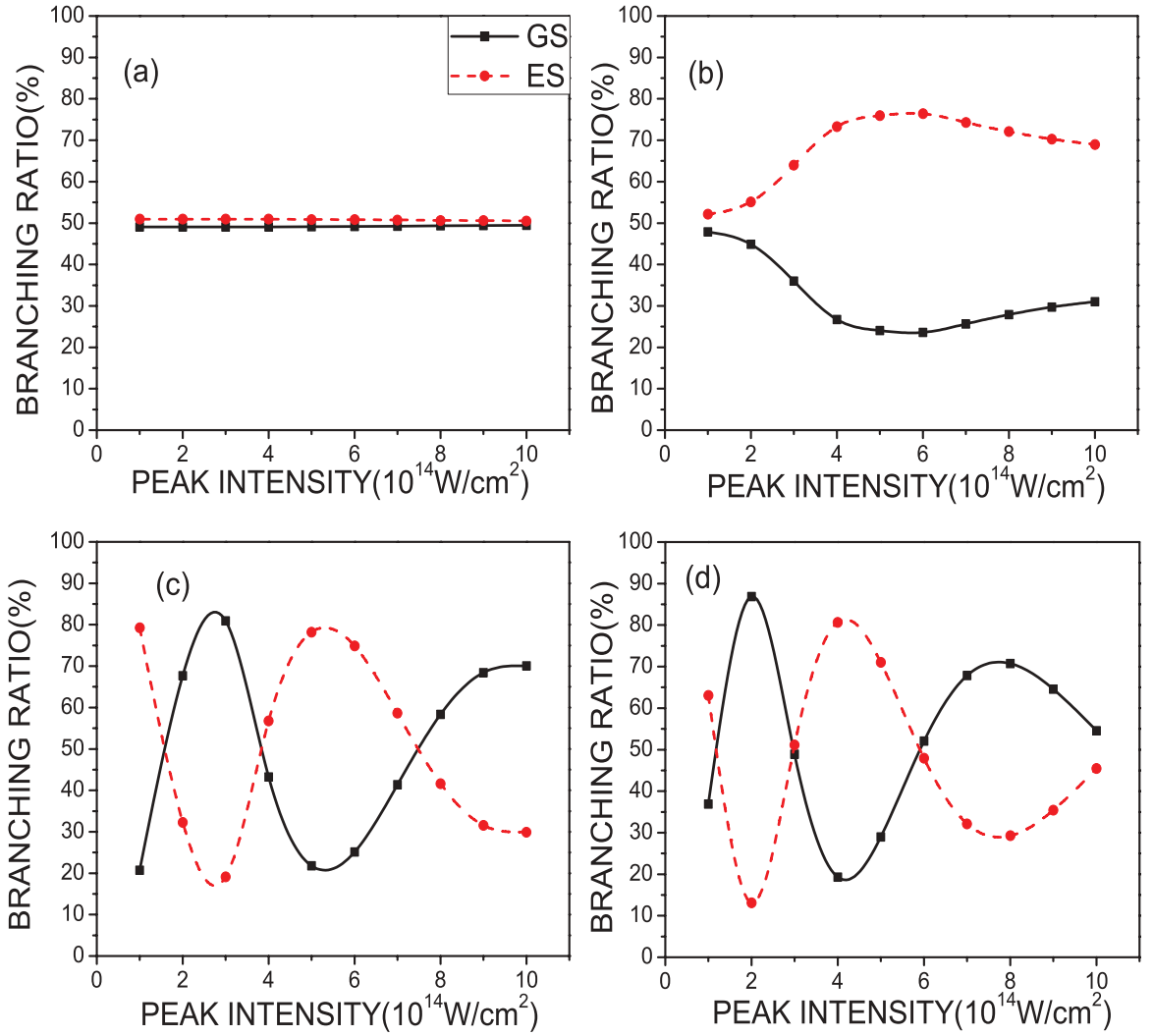

FIG. 5. (Color online) The branching ratios of the photofragments of HD^+ to the GS and ES state channel, for 267-nm-wavelength laser, as functions of intensity (I^0) for (a) $2\sigma = 24.2$ fs, (b) $2\sigma = 48.4$ fs, (c) $2\sigma = 96.7$ fs, and (d) $2\sigma = 121$ fs.

between 58 and 67 fs. Because the wave packet has moved farther right during this period the oscillations between two electronic states become damped due to the falling transition dipole moment, though some transition takes place through the nonadiabatic coupling. So we see a small decrease of the norm from the peaks in the GS and ES. For the higher intensity the decrease in the ES state is from ∼90% to ∼66% in the time interval 58–67 fs. Thus the distribution of the atomic dissociation products between the two channels is completely different at these two intensities After this time when the wave packet moves through a region of large internuclear separation (R = ∼11.5–16 a.u.) as shown in Figs. 3(g) and 3(h), the population is redistributed only between the even and odd channels within each electronic state. In this region in the absence of the nonadiabatic coupling the ES state populations would have been even lower (∼58%) at $t = 72.5$ fs. For the lower-intensity case a small rise in the GS state population starting at 62.7 fs is seen. The effect of the nonadiabatic coupling has been found to restrict transfer to the excited state.

We have found that the permanent dipole moments do play an important role in determining the branching ratio of the dissociation product between the two channels, particularly for large pulse times, for which the wave packet enters the region of large internuclear separation with the laser field remaining still operative. In such a region all the principal factors, transition dipole moments, permanent dipole moments, and nonadiabatic interaction effects are fully active while the pulse is still on and all the components of the wave packet can be simultaneously excited with transfers taking place between various pairs in varying degrees. Thus the inclusion of the permanent dipole moment opens up a large number of new pathways whose amplitudes interfere, causing a large change from the situation where the final state could be reached by a single pathway. These interference effects should cause oscillation of the branching ratio with intensity for large pulse widths. This is shown later. In this case, for both the intensities studied, the absence of the permanent dipole moments would have caused the entire dissociation flux to accumulate in the ES state reaction channel. Thus a large pulse time allows manipulation of the temporal evolution of the wave packet components on a particular potential surface and also allows influencing of the branching ratio asymmetry. In the future

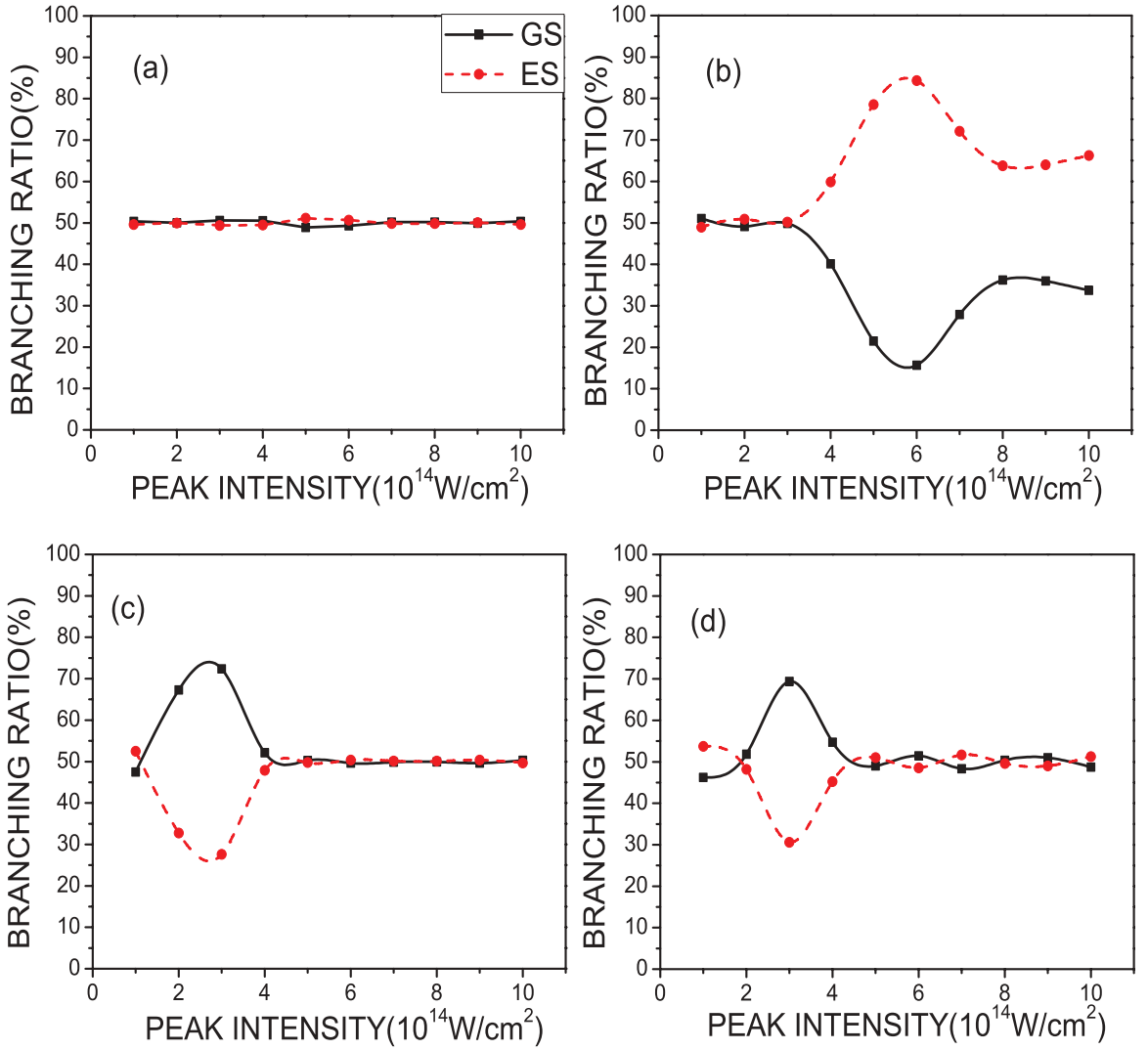

FIG. 6. (Color online) The branching ratios of the photofragments of HD^+ to the GS and ES state channel, for 800-nm-wavelength laser, as functions of intensity (I^0) for (a) $2\sigma = 24.2$ fs, (b) $2\sigma = 48.4$ fs, (c) $2\sigma = 96.7$ fs, and (d) $2\sigma = 121$ fs.

there is scope for more detailed understanding of the exact mechanism by which the permanent dipole moments affects the distribution of the flux in the two channels.

Figure 4 demonstrates the dependence of the branching ratio of the dissociated photofragments of HD^+ on the pulse time when the wavelength of the laser field used for the simulation is 800 nm. With 800-nm laser pulses, two-, three-, and four-photon dissociation all occur, their relative ratios depending on the laser parameters applied. For very low intensities, i.e., 1×10^{14}–2×10^{14} W/cm^2, substantial four-photon photodissociation is obtained. In the case of $2\sigma =$ 24.2 fs a small five-photon component is present in the final wave packet. Orr *et al.* [27] have experimentally demonstrated Above Threshold Dissociation (ATD) through the absorption of at least four photons. The experimental results presented in [28] show that for an intensity of 6×10^{14}W/cm^2 and wavelength of 800 nm, two- and three-photon dissociation processes dominate for a pulse length of 10 and 30 fs. The four-photon process was found to be more probable for pulse durations of 40 and 60 fs. The theoretical study in [29] shows that four-photon dissociation from initial ground vibrational state, and three-photon dissociation from higher levels are the most important processes. We found that for low intensities [Figs. 4(a) and 4(b)], the distribution of population in the two outgoing channels are almost equal for a certain range of pulse length (24.2–70 fs). The major difference with the 267-nm case is that here a transition to the excited electronic state in the small R region must involve a three-photon absorption process the strength of which is significantly weaker than the single-photon process relevant in the short-wavelength case. The total dissociation probability correspondingly is much smaller. Thus for lower intensities and short pulse lengths, it is mainly the nonadiabatic couplings that equalize the components of the wave packet in the $R = 10$–15 a.u. region, however small they may be. It is quite evident that in this range of pulse time, the permanent dipole moments have no significant influence on the distribution of the fragments between the two product channels. This is to be expected because for low pulse times the pulse is over by the time the wave packet reaches large distances, where the effects of large permanent dipole moments can be operative. At larger pulse times in Figs. 4(a) and 4(b), the G channel is

preferred. For higher intensities the pattern of flux distribution in the two channels against the pulse length has a remarkable resemblance to that for the 267-nm laser field, indicating a similar mechanism of differentiation between the two channels in the two cases. However, for long pulses the populations tend to equalize sooner for the 800-nm carrier wavelength.

Next we present our results, of varying the peak intensity, keeping the pulse time constant, which demonstrate the control on the branching ratio of the HD^+ photofragments exerted by the intensity. As before, the wavelengths used in our simulation consists of 267 and 800 nm for Figs. 5 and 6, respectively. The four different pulse times chosen for the simulation are 24.2, 48.4, 96.7, and 121 fs, respectively.

As is evident in Figs. 5(a) and 6(a), for a pulse duration of 24.2 fs and both wavelengths, the variation of laser intensity is not effective in causing any asymmetry in the final distribution of the dissociation products. The reason for this has already been clarified in our earlier discussion. For short pulses, the nonadiabatic coupling equalizes the distribution in the two channels in the absence of radiative interactions and the effect of the radiative coupling due to the permanent dipole moments is negligible. When the magnitude of the pulse length is doubled, as in Fig. 5(b), the wave packet is no longer confined at regions of small R during the pulse. The increased magnitudes of the radiative coupling due to the transition dipole moment, on increase of the peak intensity, effects an efficient transfer of a major fraction of the ground-state population to the excited state, creating a large asymmetry in the final distribution. When the pulse time is further increased the wave packet gets sufficient time for a cycling of the population between two states in the region where the transition dipole moment is strong. For such pulse times, an oscillatory pattern is displayed for the branching ratios with variation in intensities as seen in Fig. 5(c). As the intensity of the laser field rises, the number of oscillations between the two electronic states within a fixed time and within a given spatial region increases. The final flux distribution in the two atomic state channels depends on the phase of the oscillations within the interaction region of the two electronic potentials at the end of the pulse. At some peak intensities, for example, in the case of $2\sigma = 96.7$ fs, the population accumulates to a greater extent on the ground state for ($I^0 = 2$–3×10^{14} W/cm^2 and 8–10×10^{14} W/cm^2) but on the excited-state potentials for other intensities (e.g., $I^0 = 1 \times 10^{14}$ W/cm^2 and 4–7×10^{14} W/cm^2). As discussed earlier in the context of Figs. 3(a) and 3(e), for different pulse duration, within the same time interval the number of oscillations is greater for the high-intensity case. This leads to different population distribution in the interaction region at different intensities and eventually to different flux distribution in the two product channels in the asymptotic region. The distribution pattern presented in Fig. 5(d) is almost similar to the previous plot.

The distribution pattern, at $2\sigma = 48.4$ fs, for $\lambda = 800$ nm, on variation of peak intensity, displayed in Fig. 6(b) has similarities to that of Fig. 5(b). At the three lowest intensities the outgoing flux in the two channels are almost equal. The asymmetry in the distribution pattern for the two outgoing channels arises only from $I^0 = 4 \times 10^{14}$W/cm^2 onwards and becomes maximum at $I^0 = 6 \times 10^{14}$W/cm^2. However, unlike in Fig. 5(b), on further increase of peak intensities,

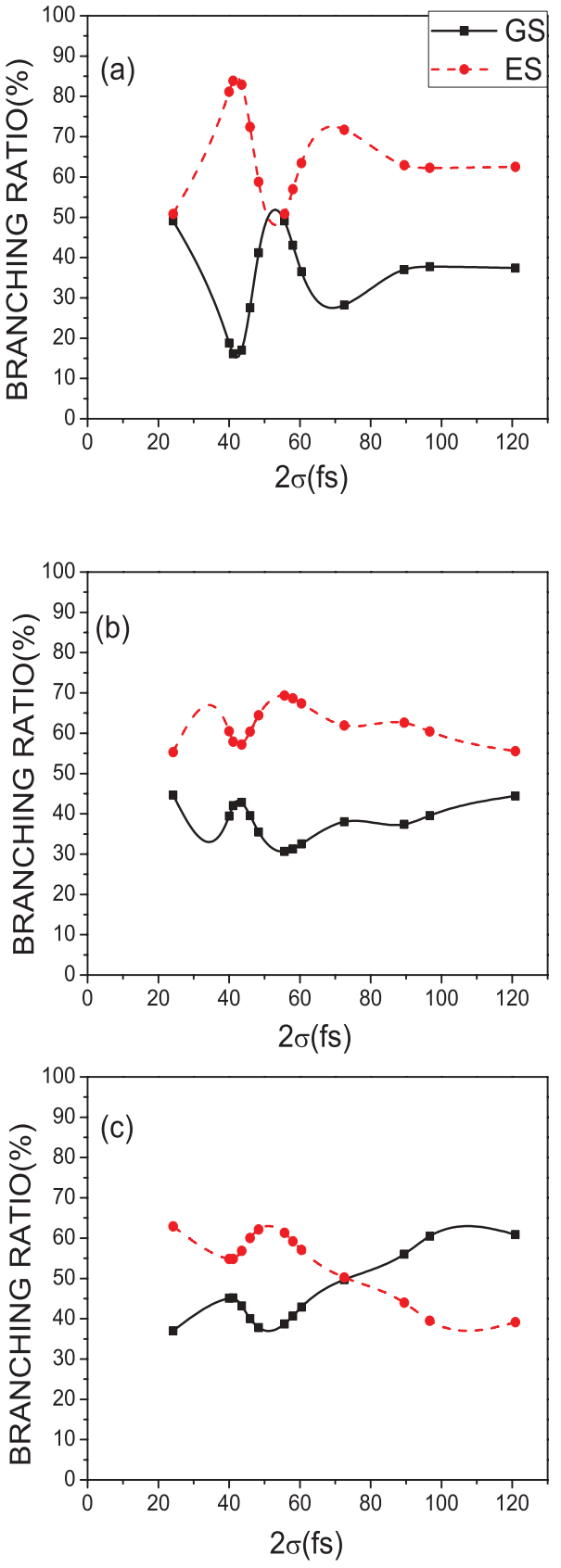

FIG. 7. (Color online) The branching ratios of the photofragments of HD^+ to the GS and ES state channel, for 267-nm-wavelength laser, as functions of pulse time (2σ) for $I^0 = 5 \times 10^{14}$W/cm^2 and different initial vibrational levels: (a) $\nu = 2$, (b) $\nu = 4$, (c) $\nu = 6$.

the population in the E channel shows some decrease with a corresponding increase in the population of the G channel. In cases of the larger pulses, as shown in Figs. 6(c) and 6(d), for 96.7 and 121 fs, respectively, an asymmetry between the G and E channel arises, only at the lower intensities where the pattern of variation is similar to the corresponding cases for a 267-nm pulse. However, the asymmetry is less in this case, possibly because for 800 nm at least a three-photon transition is necessary for the bound-state wave packet to escape to the continuum region. The population in the two channels becomes almost equal again for intensities beyond $I^0 = 4 \times 10^{14}\mathrm{W/cm^2}$. In case of the 800-nm laser pulse, the radiative couplings due to the permanent dipole moments, particularly in the high-intensity region, have a greater influence on the overall distribution of flux in the two channels. Various multiphoton transitions in the case of a low-frequency pulse allows the permanent dipole moments to play a greater role in manipulating the components of the nuclear wave packets, on the respective potentials, eventually leading to an equalization of the flux distribution in the two outgoing channels. Such transitions through involvement of the permanent dipole moments are not important for the 267-nm laser pulse.

The entire discussion so far has been based on a wave-packet propagation starting from an initial $\nu = 0$ vibrational level on the ground state potential. Figure 7 demonstrates the branching ratios as functions of pulse length for three different initial states $\nu = 2$, $\nu = 4$, and $\nu = 6$, respectively, keeping the peak intensity fixed at 5×10^{14} W/cm^2. The behavioral pattern for $\nu = 2$ in Fig. 7(a) shows that the population in the ES state channel is dominant for almost the entire range of pulse times studied. Similar features are observed for $\nu = 4$ in Fig. 7(b). However, the asymmetry in the flux distribution is slightly lower. In case of $\nu = 6$ level in Fig. 7(c) the population is predominantly in the ES state for the pulse time in the range 24.18–60.45 fs and evens out at $t = 72.54$ fs. At larger pulse times the population is in slightly higher proportion in the GS state. The initial states chosen for the simulations being multinodal, unlike that of $\nu = 0$ wave function, the radiative and nonradiative couplings may act on the wave-packet components to a different extent, thereby affecting the overall asymmetry in the branching ratio. The general effect is that the overall asymmetry shows a decrease with increasing vibrational quantum number.

IV. CONCLUSION

We have investigated the asymmetry in the branching ratios of the photofragments of the heteronuclear HD^+ molecular ion between two final atomic state channels resulting from a single femtosecond pulse from a perspective of possible control of this ratio through proper tuning of the laser parameters, e.g., laser pulse duration and peak intensity. The calculation has been performed for the fundamental frequency of a 800-nm Ti : sapphire laser and its third harmonic with a wavelength of 267 nm. We found that under some conditions a single pulse can effectively channelize the dissociated fragments into one product atomic state or another through variation of the pulse parameters. The variation of pulse times allows us to effectively control the fields when the wave-packet components pass through different regimes of radiative (both through transition and permanent dipole moments) and nonradiative (nonadiabatic coupling) interactions. This in turn can lead to change of the transition between two electronic states to different extents in different regions of space. For very low pulse times, the nonadiabatic coupling dominates and equalizes the dissociation flux in the two different channels, for a very broad range of peak intensities studied. For both the frequencies, at an intermediate pulse time, variation of intensity creates a large asymmetry in the final product distribution, with a major fraction of the flux accumulating in the ES state channel. However, in the case of a 267-nm laser, at larger pulse times, the branching ratio of the photodissociated fragments displays an oscillatory pattern with variation in laser intensities. However, for 800 nm, the asymmetry in branching, appearing at the lower intensities, completely disappears in the high-intensity regime. These variations of the branching ratio with the pulse times and intensities for different frequencies can be qualitatively interpreted in terms of the interplay between radiative and symmetry-breaking nonadiabatic interactions. We have also demonstrated the effects of the choice of initial vibrational states on the overall asymmetry in the branching ratio and found the asymmetry to be less for higher vibrational states.

ACKNOWLEDGMENT

One of the authors (S.C.) thanks the CSIR, New Delhi (Government of India) for the financial support for this work.

[1] A. Giusti-Suzor, F. H. Mies, L. F. Dimauro, E. Charron, and B. Yang, J. Phys. B **28**, 309 (1995).
[2] Th. Ergler, B. Feuerstein, A. Rudenko, K. Zrost, C. D. Schröter, R. Moshammer, and J. Ullrich, Phys. Rev. Lett. **97**, 103004 (2006).
[3] M. V. Korolkov and K.-M. Weitzel, J. Chem. Phys. **123**, 164308 (2005).
[4] M. V. Korolkov, H. G. Breunig, and K.-M. Weitzel, Opt. Spectrosc. **103**, 325 (2007).
[5] H. G. Breunig, A. Lauer, and K.-M. Weitzel, J. Phys. Chem. A **110**, 6395 (2006).
[6] J. L. Herek, A. Materny, and A. H. Zewail, Chem. Phys. Lett. **228**, 15 (1994).
[7] C. J. Bardeen, J. Che, K. R. Wilson, V. V. Yakovlev, P. Cong, B. Kohler, J. L. Krause, and M. Messina, J. Phys. Chem. A **101**, 3815 (1997).
[8] B. H. Hosseini, H. R. Sadeghpour, and N. Balakrishnan, Phys. Rev. A **71**, 023402 (2005).
[9] E. Charron and A. Suzor-Weiner, J. Chem. Phys. **108**, 3922 (1998).
[10] S.-M. Wang, K.-J. Yuan, Y.-Y. Niu, Y.-C. Han, and S.-L. Cong, Phys. Rev. A **74**, 043406 (2006).

[11] D. G. Abrashkevich, M. Shapiro, and P. Brumer, J. Chem. Phys. **108**, 3585 (1998).
[12] Y.-C. Han, K.-J. Yuan, W.-H. Hu, T.-M. Yan, and S.-L. Cong, J. Chem. Phys **128**, 134303 (2008).
[13] M. Sukharev, E. Charron, and A. Suzor-Weiner, Phys. Rev. A **66**, 053407 (2002).
[14] J. J. Hua and B. D. Esry, Phys. Rev A **80**, 013413 (2009).
[15] E. Charron, A. Giusti-Suzor, and F. H. Mies, J. Chem. Phys. **103**, 7359 (1995); Phys. Rev. Lett. **75**, 2815 (1995).
[16] I. Ben-Itzhak, E. Wells, K. D. Carnes, V. Krishnamurthi, O. L. Weaver, and B. D. Esry, Phys. Rev. Lett. **85**, 58 (2000).
[17] E. Wells, B. D. Esry, K. D. Carnes, and I. Ben-Itzhak, Phys. Rev. A **62**, 062707 (2000).
[18] V. Roudnev, B. D. Esry, and I. Ben-Itzhak, Phys. Rev. Lett. **93**, 163601 (2004).
[19] V. Roudnev and B. D. Esry, Phys. Rev. A **76**, 023403 (2007).
[20] R. Bhattacharya and S. S. Bhattacharyya, Phys. Rev. A **79**, 043415 (2009).
[21] B. Dutta, S. Sen, S. Saha, and S. S. Bhattacharyya, Phys. Rev. A **68**, 013401 (2003).
[22] B. Dutta, R. Bhattacharya, and S. S. Bhattacharyya, Phys. Rev. A **80**, 043413 (2009).
[23] F. He, C. Ruiz, and A. Becker, Phys. Rev. Lett. **99**, 083002 (2007).
[24] C. R. Calvert, R. B. King, W. A. Bryan, W. R. Newell, J. F. McCann, J. B. Greenwood, and I. D. Williams, J. Phys. B **43**, 011001 (2010).
[25] A. Carrington and R. A. Kennedy, Mol. Phys. **56**, 935 (1985).
[26] R. E. Moss and I. A. Sadler, Mol. Phys. **61**, 905 (1987).
[27] P. A. Orr, I. D. Williams, J. B. Greenwood, I. C. E. Turcu, W. A. Bryan, J. Pedregosa-Gutierrez, and C. W. Walter, Phys. Rev. Lett. **98**, 163001 (2007).
[28] J. D. Alexander *et al.*, J. Phys. B **42**, 154027 (2009).
[29] B. A. Song-Yue, Y. Kai-Jun, H. Yong-Chang, and C. Shu-Lin, Chin. Phys. Lett. **25**, 2845 (2008).